THE JOURNAL OF PHYSICAL CHEMISTRY C

pubs.acs.org/JPCC Article

Naphthalenediimide Cations Inhibit 2D Perovskite Formation and Facilitate Subpicosecond Electron Transfer

Andrew H. Proppe, Marie-Hélène Tremblay, Yadong Zhang, Zhenyu Yang, Rafael Quintero-Bermudez, Shana O. Kelley, Stephen Barlow, Seth R. Marder, and Edward H. Sargent*

Cite This: https://dx.doi.org/10.1021/acs.jpcc.0c05521 Read Online

ACCESS | Metrics & More | Article Recommendations | Supporting Information

ABSTRACT: Layered metal halide perovskites, also called perovskite quantum wells (PQWs), are versatile optoelectronic materials possessing large oscillator strengths, band gaps tuned via the quantum size effect, and promising stability. The majority of examples of PQWs make use of small aryl- and alkylammonium A′-site cations to tune dimensionality and stability, with fewer examples of larger molecules that exhibit frontier orbital energies near those of the inorganic component of the perovskite. Here, we report two new lead-iodide-based systems that incorporate a dye molecule A′-site dication, 2,2′-[naphthalene-1,8:4,5-bis(dicarboximide)-*N*,*N*′-diyl]-bis(diethylammonium) (NDIC2), along with either methylammonium or a mixture of methylammonium and formamidinium as A-site cations. From transient absorption spectra, we find that films synthesized with NDIC2, PbI_2, and methylammonium inhibit the growth of PQWs and instead result in a mixture of weakly confined perovskite and 1D perovskitoid structures. When both formamidinium and methylammonium are used as A-site cations, we observe spectroscopic signatures of quantum-confined 2D structures similar to PQWs with a polydisperse well width distribution. We observe a rapid (∼700 fs) decay of the photoexcited perovskite carrier population in the presence of NDIC2 and fully quenched photoluminescence: this is consistent with ultrafast perovskite-to-NDIC2 electron transfer. This work explores the interplay between large and small cation molecules in influencing the perovskite structure and how such molecules may offer a route to structures with charges separately localized on inorganic and organic components, raising prospects of using perovskites with electron-accepting ligands for hybrid organic–inorganic optoelectronic devices.

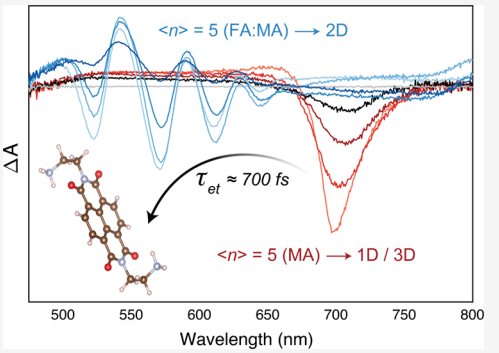

INTRODUCTION

Metal halide perovskites have advanced rapidly as solution- and vacuum-processed materials for optoelectronics.[1−7] Two-dimensional analogues of these materials—known as perovskite quantum wells (PQWs)—have emerged as a materials platform exhibiting increased stability over 3D analogues,[1,8,9] band gaps tunable via variable quantum and dielectric confinement,[10−14] and electronic structures with similarities to quantum well materials.[15−18] However, compared to all-inorganic quantum well materials such as GaAs and InGaAs, PQWs feature much greater chemical diversity: their properties are influenced by the choice of organic cations used to synthesize the wells, and this affects polydispersity, interwell coupling, energy and charge transfer efficiencies, and overall carrier mobilities.[8,10,19−23] Quantum-confined perovskite and perovskitoid structures with further reduced dimensionality, such as quantum wires (1D) and quantum dots (0D), have also been studied.

In 2D PQW systems, large organic cations (hereafter referred to as A′-site cations) are used to terminate the perovskite lattice along one axis, resulting in a quantized number of perovskite monolayers, indicated by an integer *n*, that are confined between molecular bilayer interfaces. These bulky molecules typically contain terminal NH_3^+ groups that replace smaller A-site cations, such as methylammonium (MA) and formamidinium (FA), and can fit into cuboctahedral sites in the bulk perovskite lattice. Although in some cases pure crystals defined by a single *n* value can be achieved,[12,24] thin films of PQWs typically form with a distribution of well widths centered around the designated *n* value, ⟨*n*⟩—the quantum well width expectation value. A′-site cations conventionally used to form PQWs are alkyl- and arylammonium molecules, which in thin films typically yield a polydisperse well-width (and band gap) distribution. This can improve the photoluminescence quantum yield by forming an energy gradient between the wells, favoring energy transfer.[16,23,25,26] Despite interwell distances on the order of 1 nm using these insulating

Received: June 17, 2020
Revised: September 10, 2020

molecules, interwell charge transfer still occurs with appreciable efficiencies on subnanosecond timescales,[23,27] facilitating the operation of PQW-based photovoltaics with solar power conversion efficiencies in the range of 12−18%.[1,8,9,21,22]

A domain as yet underexplored in PQW chemistry is the use of A′-site cations that possess frontier molecular orbitals that can electronically couple to the perovskite conduction or valence bands. Seminal work by Mitzi et al. demonstrated such a hybrid material consisting of PQWs using oligothiophene cations that formed type-I heterostructures.[28] Charge injection from the PQWs into the oligothiophene was favored, facilitating electroluminescence from the organics in light-emitting diodes.[29] Passarelli et al. showed that large perylene A′-site cations can enhance the stability of purely 2D (n = 1) PQWs, allowing them to survive full immersion in water and improving out-of-plane conductivity through favorable alignment of the organic frontier orbitals and the PQW bandedge.[30] Gélvez-Rueda et al. demonstrated colloidal perovskite nanoplatelets using perylenediimide ligands, where a type-II band alignment enabled ultrafast charge separation between the perovskite and the perylenediimide molecules.[31] More recently, doping of pyrene- and naphthalene-based A′-site cation organic layers was used to form charge-transfer complexes; in the latter case, these interactions could be used to tune the 1 s exciton binding energy of n = 1 PQWs.[32,33] In thin films, the utility of such A′-site cations has been demonstrated in 0D, 1D, and 2D perovskite-like structures, but not yet in higher n (i.e., quasi-2D) PQWs; however, these are typically required for efficient photovoltaic and light-emitting devices.

Here, we pursued PQW thin films that incorporate a bridging A′-site dication naphthalene diimide (NDI), 2,2′-[naphthalene-1,8:4,5-bis(dicarboximide)-N,N′-diyl]-bis-(ethylammonium),[34] functionalized at opposite ends using ethylammonium groups in order to form a bridge between two neighboring wells, which we term NDIC2. NDI molecules are of potential interest for use as cations for PQWs owing to their facile synthesis and their planar structure, and have been incorporated in hybrid 1D and 2D perovskite-like structures which consist solely of PbI_2, additional iodide ions, and NDI-based cations.[35−37] A recent study demonstrated numerous 0D and 1D structures formed from PbI_2 and NDIC2, where the structures could be altered by crystallization conditions or thermal- and solvent-induced transformations.[38] However, no 2D PQW structures or materials including both NDIC2 and other organic cations have yet been reported. We fabricated thin films of higher n perovskites containing NDIC2 molecules to study how they affect PQW formation, width distribution, structure, spatial ordering, and photoexcited carrier dynamics of the hybrid system.

EXPERIMENTAL METHODS

NDCI2 Synthesis. 2,2′-Naphthalene-1,8:4,5-bis-(dicarboximide)-N,N′-diyl]-bis(ethyammonium) diiodide (NDIC2-I_2) was synthesized according to our recent report.[38] 4,4′-Naphthalene-1,8:4,5-bis(dicarboximide)-N,N′-diyl]-bis-(butylammonium) diiodide (NDIC4-I_2) was synthesized in an analogous fashion, but we found that this salt was poorly soluble in DMF and DMSO, preventing us from coating sufficiently thick films for optical and structural characterization.

Sample Preparation. All films were deposited onto glass or patterned ITO on glass substrates that were first cleaned by sequential sonication for 15 min in baths of acetone and isopropanol, and then dried under a nitrogen flow and treated with oxygen plasma for 10 min prior to spin-coating.

NDIC2-based perovskite thin films were prepared in a nitrogen glovebox by dissolving different ratios of methylammonium iodide (MAI, 111.97 $gmol^{-1}$), formamidinium iodide (FAI, 171.97 $gmol^{-1}$), naphthalenediimide diethylammonium (NDIC2, 608.17 $gmol^{-1}$), and lead(II) iodide (PbI_2, 461.0 $gmol^{-1}$) in DMF. Table S1 in the Supporting Information provides the exact amounts of each precursor dissolved in 1 mL of DMF in order to give a 0.8 M solution (based on concentration of Pb^{2+}).

The solutions were then transported into another (solvent-free) nitrogen glovebox and stirred at 70 °C for a minimum of 1 h before being passed through a PTFE filter (0.22 μm), and 70 μL of this precursor solution was dropped onto a glass substrate and spun at 4000 rpm for 20 s. The substrate was then placed on a hotplate set to 100 °C to anneal for 15 min.

X-ray Diffraction. XRD patterns were obtained using a Rigaku MiniFlex 600 diffractometer (Bragg−Brentano geometry) equipped with a NaI scintillation counter detector and a monochromatized Cu Kα radiation source (λ = 1.5406 Å) operating at a voltage of 40 kV and current of 15 mA.

UV−Vis Absorption Measurements. Thin-film absorption measurements were carried out in a Lambda 950 UV−vis−IR spectrophotometer (PerkinElmer).

Photoluminescence Measurements. Photoluminescence measurements were performed using a Horiba Fluorolog time-correlated single photon counting (TCSPC) system with photomultiplier tube detectors. A pulsed laser diode (374 nm, 110−140 ps pulse width) was used as an excitation source.

Ultrafast Transient Absorption Spectroscopy. Ultrafast pulses of a 1030 nm fundamental beam with a 5 kHz repetition rate were produced using a regeneratively amplified Yb/KGW laser (PHAROS, Light Conversion). One part of the fundamental beam was used to pump an optical parametric amplifier (ORPHEUS, Light Conversion) to serve as a narrowband pump, and the other part was focused into a sapphire crystal in order to generate a white light continuum probe in the range of ∼475−850 nm. Both pulses were directed into a commercial transient absorption spectrometer (Helios, Ultrafast). The probe pulse was delayed relative to the pump pulse using a delay stage that provided a time window of up to 8 ns.

Ultraviolet Photoelectron Spectroscopy. Measurements were performed with an Escalab Xi + Microprobe system equipped with a He 1α source, with a spot size of 2.5 mm and energy steps of 0.02 eV. Film samples were spun on glass substrates patterned with ITO, and a corner of the film was scratched where electrically conductive carbon tape was adhered to avoid charging. All UPS measurements were conducted with a 5 V bias.

Single-Crystal X-ray Diffraction. Data were collected on a Bruker Kappa APEX-DUO diffractometer using monochromated Mo-Kα radiation (Bruker Triumph) equipped with a CCD detector and were measured using a combination of ϕ scans and ω scans. The data were processed, and absorption corrections were carried out using APEX2, SAINT, and SADABS (Bruker). The structures were solved with SHELXT[39] and refined using SHELXL[40] for full-matrix least-squares refinement that was based on F^2. H atoms were included in calculated positions and allowed to refine in riding-motion approximation with U_{iso} tied to the carrier atom. The

https://dx.doi.org/10.1021/acs.jpcc.0c05521
J. Phys. Chem. C XXXX, XXX, XXX−XXX

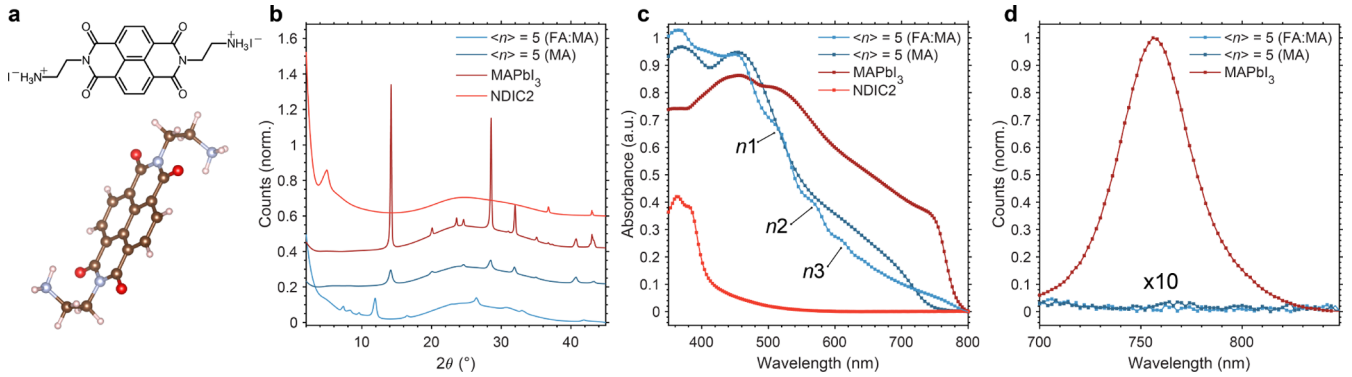

Figure 1. (a) Structure of the naphthalenediimide diethylammonium (NDIC2) dication used in this work. (b) XRD patterns, normalized and offset for clarity. All films were spin-coated onto glass slides for characterization. (c) Absorbance spectra for the thin films with solution precursor stoichiometries of $\langle n \rangle = 5$ (FA/MA), formula (NDIC2) $(FA_{0.85}MA_{0.15})_4Pb_5I_{16}$; $\langle n \rangle = 5$ (MA), formula (NDIC2)$MA_4Pb_5I_{16}$; $MAPbI_3$; and a spin-coated film of the NDIC2 dication. Features in the $\langle n \rangle = 5$ (FA/MA) spectrum are tentatively assigned as $n = 1$, 2, and 3 PQWs and labeled as such based on literature values.[10,23] (d) Photoluminescence (PL) spectra. Spectra for the $\langle n \rangle = 5$ films are magnified 10-fold.

crystal structure data may be obtained in CIF format from the Cambridge Crystallographic Data Center (www.ccdc. cam.a-c.uk), with deposition number CCDC 2010470.

RESULTS AND DISCUSSION

Films were spin-coated onto glass substrates from a precursor DMF solution consisting of NDIC2-I_2, PbI_2, and MAI with or without FAI (see Experimental Methods). Because our goal was to synthesize 2D PQW structures (the general formula for which is $A'_2A_{n-1}Pb_nI_{3n+1}$, where A′ is a large monocation and A is a small cation that can fit in a cuboctahedral site), the precursor ratios in solution were chosen to correspond to an $\langle n \rangle$ value according to the formula (NDIC2) $(MA/FA)_{n-1}Pb_nI_{3n+1}$ (because NDIC2 is dicationic). The molecular structure of NDIC2 is shown in Figure 1a, alongside X-ray diffraction (XRD) patterns, absorption spectra, and photoluminescence (PL) spectra (panels a, b, and c, respectively) for thin films with NDIC2, FA, and MA cations used in ratios corresponding to $\langle n \rangle$ values of 5 and ∞ (i.e., $MAPbI_3$), as well as a spin-coated film of NDIC2-I_2. We chose $\langle n \rangle = 5$ because this formula has been used with short-chain cations to prepare thin film layers in efficient photovoltaic and LED devices. The $MAPbI_3$ thin film serves as a reference for the purely 3D perovskite semiconductor that does not experience quantum/dielectric confinement.

The $\langle n \rangle = 5$ (FA/MA) films were coated using a mixture of FA/MA in a ratio of 85:15 [(NDIC2) $(FA_{0.85}MA_{0.15})_4Pb_5I_{16}$], whereas the precursor mixtures for the $\langle n \rangle = 5$ (MA) films contained only MA and no FA [(NDIC2) $(MA_4)Pb_5I_{16}$]. To confirm the presence of NDIC2 in the films, they were redissolved in DMSO-d_6 for ^{1}H NMR measurements, from which we obtained NDIC2:MA:FA ratios of ∼1:5:0 and ∼1:1:4 for the $\langle n \rangle = 5$ (FA/MA) and $\langle n \rangle = 5$ (MA) films, respectively (Figures S1 and 2). This indicates that the FA/MA ratio is ∼80:20 rather than 85:15 as in the precursor solution mixture. In both cases, the ratios between NDIC2 and the MA and FA cations correspond to the ratio expected for PQWs with $\langle n \rangle$ values of 6, instead of 5, although without also knowing the ratios of the cations relative to Pb and I, we cannot assign a formula to the film. We have previously observed similar deviations of the film stoichiometry from that of the precursor solution, which depended on the A′-site cation used.[22] For simplicity, we continue to the refer to the film $\langle n \rangle$ as that of the solution stoichiometry, while noting that these feed ratios may not directly translate to the films. The ^{1}H NMR spectra also revealed that some of the DMF solvent was retained in the thin films, despite thermal annealing at 100 °C for 15 min (Figure S3).

The XRD pattern for the $\langle n \rangle = 5$ (FA/MA) film shows a series of peaks between $2\theta \approx 7-11°$, which may correspond to PbI_2 (11°) and precursor complexes, but otherwise does not show any peaks originating from low-n PQWs or bulk 3D perovskite (14°). This is in contrast to the multiple low-angle peaks that are usually present in $\langle n \rangle = 5$ films prepared using conventional alkylammonium cations such as phenethylammonium (PEA) or butylammonium (BTA),[41] indicating that if PQWs form in the NDIC2/FA/MA case, they are highly disordered by comparison. In the absence of FA, $\langle n \rangle = 5$ (MA), a diffraction peak corresponding to the (110) peak of $MAPbI_3$ is observed at 14°. Moreover, in some cases, a broad and weak diffraction centered at ∼8° is observed, which can be assigned to a 1D structure (vide infra).

We observe that the absorption profile of the $\langle n \rangle = 5$ (MA) film has a blue-shifted bandedge compared to $MAPbI_3$, but no discernible exciton resonances for low-n PQWs. Previously reported 1D crystal structures containing Pb, I, and NDIC2 exhibited a similar absorption onset, which was hypothesized to be due to charge transfer,[38] and could explain the absorption profile of our $\langle n \rangle = 5$ (MA) film if similar structures have been formed. Alternatively, the blue-shifted bandedge could be indicative of quantum confinement effects, for example, if another type of quantum-confined structure had been formed instead of a 2D PQW. In the $\langle n \rangle = 5$ (FA/MA) films, where 80% of the MA molecules are replaced by FA, we instead observe several peaks at wavelengths corresponding to exciton absorption of $n = 1$ (515 nm), 2 (570 nm), and 3 (610 nm) PQWs,[41] which are more clearly identified using transient absorption spectroscopy (see below). Because there are no other A′ cations present, this suggests that the NDIC2 molecules may be able to induce the formation of PQWs. Compared to $MAPbI_3$, there is also pronounced absorption between 350 and 400 nm in both $\langle n \rangle = 5$ thin films, which likely originates from the absorption peak of the NDIC2 molecule in the same spectral region. Considering the excitonic features which are consistent with 2D structures being present in the $\langle n \rangle = 5$ (FA/MA) thin film and the lack of any observable XRD peaks corresponding to these well widths, we

https://dx.doi.org/10.1021/acs.jpcc.0c05521
J. Phys. Chem. C XXXX, XXX, XXX−XXX

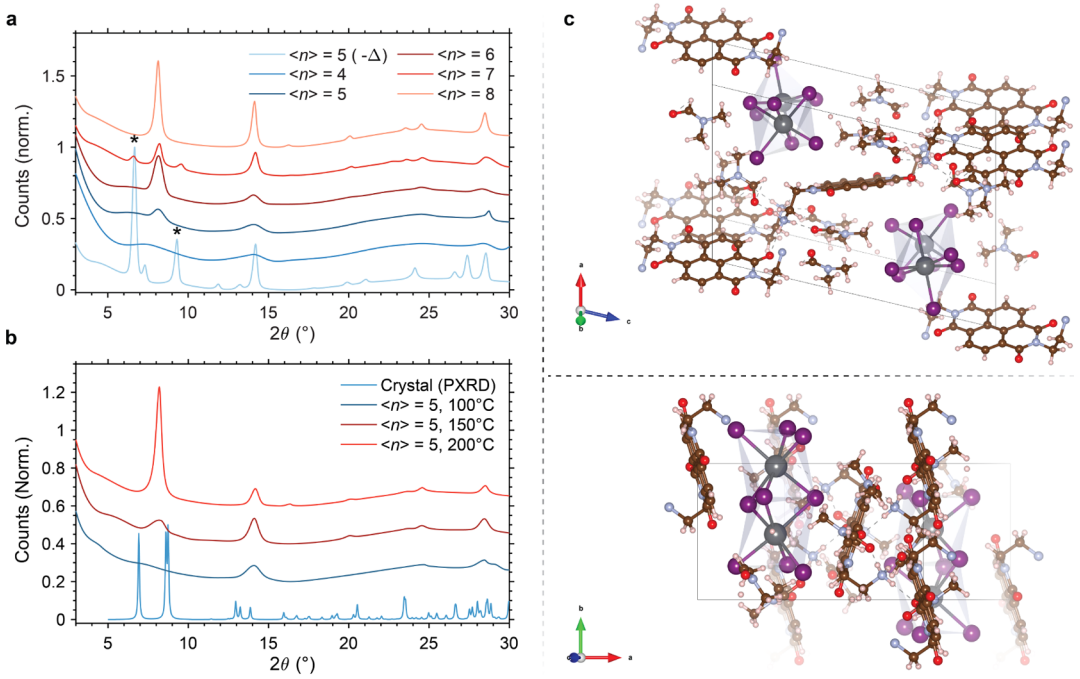

Figure 2. (a) XRD patterns for $\langle n \rangle$ = 4−8 (MA) films. The (−Δ) indicates that the film was not annealed after spin-coating. The * labels peaks originating from precursor complexes. (b) Simulated powder XRD pattern for the crystal structure shown in panel c, and XRD patterns for $\langle n \rangle$ = 5 films annealed at 100, 150, and 200 °C. (c) Crystal structure of an NDIC2-PbI_2-DMF complex with formula $(NDIC2)Pb_2I_6 \cdot 4(DMF)$. Crystals were grown with a precursor stoichiometry corresponding to n = 1, $(NDIC2)PbI_4$, in a DMF solvent.

posit that there could be limited spatial coherence between the wells resulting from disorder, which prevents strong diffraction.

The PL emission (Figure 1d) for both $\langle n \rangle$ = 5 films are completely quenched compared to the $MAPbI_3$ thin film under identical excitation conditions (no signal was detected at wavelengths corresponding to the higher energy peaks in the FA/MA thin film). PQW thin films with polydisperse well width distributions often show enhanced PL quantum yield as a result of rapid energy transfer from larger to smaller band gap wells.[23,25,26] If PQWs have formed, the quenched rather than enhanced emission in our films is therefore attributable to the presence of the NDIC2 molecules. We hypothesize later in this work that this complete elimination of PL is due to charge separation between the PQWs and NDIC2, as has been observed in 0D, 1D, and 2D NDI-PbI_2 hybrid structures,[35−37] and more recently in colloidal perylenediimide-PQW structures.[31]

To try and clarify the structure of the materials using only MA and NDIC2 as cations, we prepared a series of films with $\langle n \rangle$ = 4−8, along with one $\langle n \rangle$ = 5 film that was not thermally annealed, and collected XRD patterns (Figure 2a). We also collected patterns for $\langle n \rangle$ = 5 films annealed at different temperatures (Figure 2b). The patterns all show two main peaks: one at 2θ = 14°, corresponding to the (110) peak of $MAPbI_3$ and another at 2θ = 8°. The XRD pattern for an $\langle n \rangle$ = 5 film that was not annealed shows two peaks at 6.5 and 9°. To characterize the structure of these materials, we attempted, using a slow solvent diffusion crystallization method, to grow single crystals of purely 2D (n = 1) PQWs using the NDIC2 dication.[42] Single-crystal structures of 2D PQWs have been obtained for monocation and dication A′-site molecules, which usually yield either Ruddlesden-Popper[10,12] or Dion-Jacobsen[43] phases, respectively. Instead of PQWs, we obtained perovskitoid 1D chains of face-sharing Pb/I octahedra surrounded by DMF solvent molecules and NDIC2, similar to those found in ref 38, where many of those structures also contained solvent molecules. A view of the structure is shown in Figure 2c. The simulated powder diffraction pattern of this 1D perovskitoid has 2 peaks (6.5 and 9°, Figure 2b) that corresponds to the un-annealed film. Once annealed, these peaks are replaced by one at 8°. The peak at 8°, rather than being eliminated upon heating, instead becomes more intense when the annealing temperature is raised from 100 to 200 °C, even as the (110) peak of $MAPbI_3$ begins to diminish. Peaks in the range of $2\theta \approx 8°$ have been observed in 1D PbI_2-NDI nanowires and coordination polymer hybrids,[36,37] and for the PbI_2/NDIC2-I_2 structures from ref 38, leading us to believe that similar structures may be formed in our (NDIC2)-$MA_{(n-1)}Pb_nI_{3n+1}$ films upon annealing. We posit that the formation of similar 1D-like structures is favored over the formation of low-n PQW structures, both in single crystal growth and in spin-coating of thin films, although the structures in thin films may also incorporate MA (which is absent from the crystal growth solutions). We note that it is not uncommon for 1D structures to form in single crystals from mixtures of large organic ammonium cations and lead halide salts; but to the best of our knowledge, this is rarely observed during spin-coating of thin films in the presence of smaller A-site cations like MA or FA, and typically quasi-2D PQW structures are obtained instead. This could result from stronger interactions between, and lower solubility of, the planar conjugated NDIC2 cations compared to conventional A′ cations, suggesting a templating effect of the NDIC2 that favors the formation of 1D structures.

We hypothesize that in the absence of FA, the thin films form as a mixture of quasi-3D perovskite and 1D structures interspersed throughout, possibly consuming NDIC2 and inhibiting low-n PQW formation. This is consistent with the

https://dx.doi.org/10.1021/acs.jpcc.0c05521
J. Phys. Chem. C XXXX, XXX, XXX−XXX

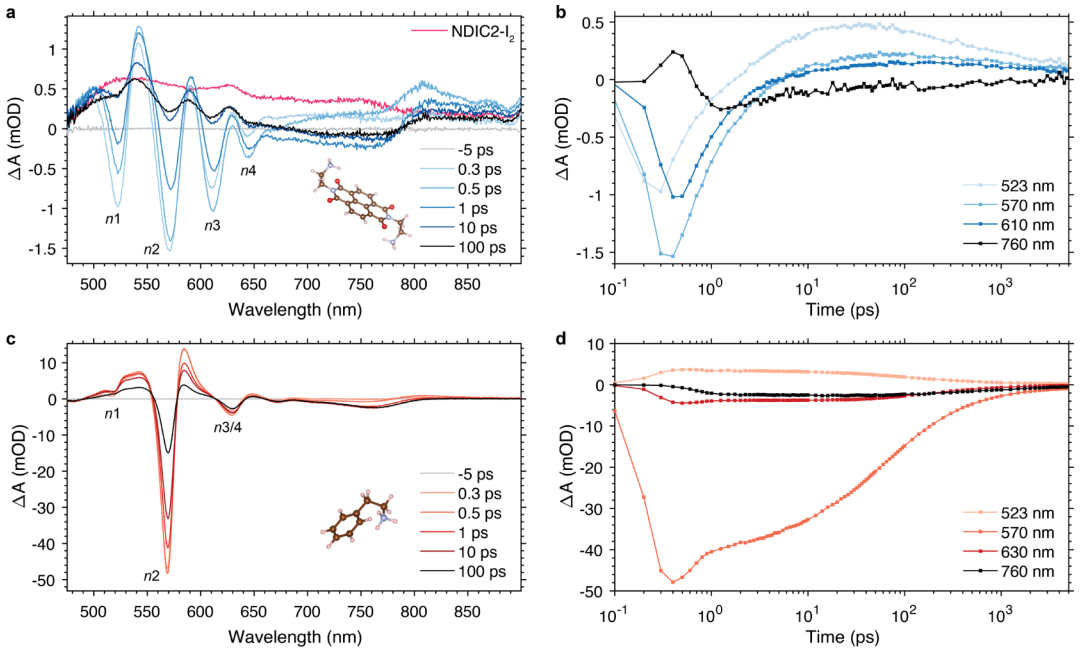

Figure 3. (a) Transient absorption spectra at delay times between −5 and 100 ps for the $\langle n \rangle$ = 5 (FA/MA) thin film. The transient absorption spectrum for a thin film of NDIC2-I_2 at a delay time of 1 ps is shown in pink. Exciton peaks for n = 1−4 PQWs are labeled according to literature values.[23] (b) Kinetic traces drawn from wavelengths corresponding to n = 1, 2, 3, and ∞ (3D). (c) Transient absorption spectra and (d) kinetic traces for an $\langle n \rangle$ = 3 thin film using PEA as A′. All experiments were performed with an excitation wavelength of 450 nm and a pump fluence of ∼0.1 mJ/cm^2. The peak labeled n3/4 in the PEA-based film is at a wavelength that is intermediate between what is normally expected for n = 3 (610 nm) and n = 4 (640 nm) PQWs in TA spectra,[23,44] which we speculate results from mixing of the FA and MA cations. The bleach peak positions, dynamics, and PQW distribution in this film are very similar to other examples from literature.[23,25]

XRD patterns of all the (NDIC2)$MA_{(n-1)}Pb_nI_{3n+1}$ films showing one peak at 8°, likely corresponding to a 1D structure, and at 14°, corresponding to $MAPbI_3$. The presence of these 1D structures in thin films is further supported by the aforementioned ^{1}H NMR measurements of (NDIC2)-$MA_{(n-1)}Pb_nI_{3n+1}$ films, which revealed that DMF is still present in the thin films, even after thermal annealing, and so may be incorporated into the crystal structure (Figure S3).

The increasing intensity of the 2θ = 8° XRD peak with higher thermal annealing temperatures (Figure 2b) is consistent with the evaporation of volatile MA from the material, leaving the remaining components to assemble into 1D structures. The behavior with increasing annealing temperature also indicates that the 1D structure is relatively stable (compared to $MAPbI_3$) under thermal stress and does not decompose within the 15 min annealing times used here; consistent with the retention of DMF despite its volatility.

We next used ultrafast transient absorption (TA) spectroscopy to study the photoinduced carrier dynamics of the NDIC2 perovskite thin films. We began with the $\langle n \rangle$ = 5 (FA/MA) film owing to the appearance of peaks in the absorption spectrum at wavelengths corresponding to low-n PQWs. The photoexcitation wavelength was set to 450 nm to ensure that all perovskite structures present could be populated by the pump pulse. We also attempted experiments using a pump wavelength of 380 nm to resonantly photoexcite NDIC2 such that we could potentially observe carrier transfer to the perovskite structures. However, we found that the perovskite itself exhibited a bleach peak that overlapped significantly with that of the NDIC2 molecules (Figure S4). We observed some subpicosecond amplitude exchange from the NDIC2 peak to the perovskite, possibly arising because of ultrafast exciton or electron/hole transfer (Figure S5); however, because of the high degree of overlap between these peaks, in addition to the instability of our white light spectrum at UV wavelengths and poor signal-to-noise ratios resulting from limited film thickness (due to the solubility of the NDIC2 salt), a definite picture of any population transfer was not available to us.

We instead focused on the carrier dynamics of the directly photoexcited perovskites in a probe range of 475−900 nm. As a control, we also fabricated FA/MA PEA-based $\langle n \rangle$ = 3 thin films with nominal formula $PEA_2(FA_{0.85}MA_{0.15})_2Pb_3I_{10}$. An $\langle n \rangle$ of 3 instead of 5 was chosen because this resulted in a spectral distribution more similar to the NDIC2-based thin films. TA spectra at delay times ranging between −5 and 100 ps for both of these thin films are shown in Figure 3a,c. At early delay times, signals that are strongly reminiscent of the exciton resonances for PQWs of $\langle n \rangle$ = 1−4 are clearly visible in both films. Compared to PEA (Figure 3c), the NDIC2-based films show pronounced positive amplitude over the entire spectral range (Figure 3a), consistent with the population of NDIC2, whose TA spectrum at a delay time of 1 ps (using a pump wavelength of 380 nm) is superimposed on traces from the $\langle n \rangle$ = 5 (FA/MA) films. NDIC2 spectra at other delay times are shown in Figure S6. The photoexcited NDIC2 produces substantial photoinduced absorption (PIA) signals, which are similar to the expected spectrum of an $NDI^{\bullet-}$ radical anion (negative-going bleach signals from the NDI are not captured in this spectral range by our white light probe, but are observable at UV wavelengths; see Figure S4).[45−47] When NDIC2 is in close proximity to the perovskite lattice or incorporated as an A′-site cation, it could enable photoinduced electron transfer from the PQWs to NDIC2. We note that in the absence of any perovskite (thin films of only NDIC2-I_2), this could also indicate that there is photoinduced electron transfer from iodide to the NDIC2 cation.[48] The prominent

https://dx.doi.org/10.1021/acs.jpcc.0c05521
J. Phys. Chem. C XXXX, XXX, XXX−XXX

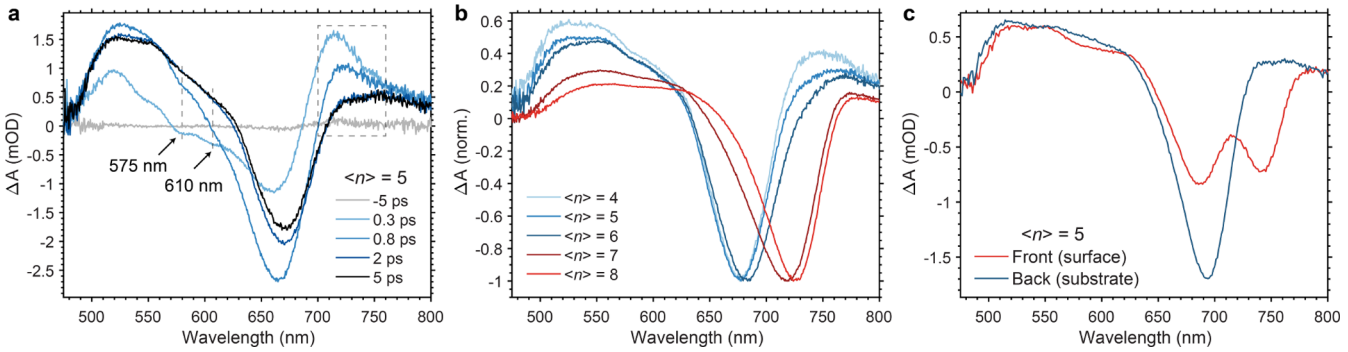

Figure 4. (a) TA spectra for an $\langle n \rangle = 5$ (MA) film at various delay times. The dashed gray box highlights the lower energy PIA that decays within the first few ps. The arrows point to bleach peaks at ∼575 and ∼610 nm, which also decay within the first few ps. (b) TA spectra for $\langle n \rangle = 4-8$ (MA) NDIC2-based thin films, and (c) for an $\langle n \rangle = 5$ film prepared using a precursor solvent mixture of DMSO/GBL, with laser pulses impinging on the front (surface) and back (substrate) sides of the film. Spectra shown in panels b and c are taken at a delay time of 2 ps, and all experiments were performed with an excitation wavelength of 450 nm and a pump fluence of ∼0.1 mJ/cm^2.

spectral features between 500 and 650 nm are slightly different than those observed in TA spectra of neat NDI or in the steady-state spectra for typical NDI anions, which could be due to effects of NDI−NDI aggregation that might broaden or shift the features. We thus tentatively propose $NDI^{\bullet-}$ as the origin for the PIA signals observed in the PQW-NDIC2 hybrid thin films.

In the absence of other A′-site molecules in the $\langle n \rangle = 5$ (FA/MA) film, the TA spectra further support that NDIC2 is able to induce the formation of PQWs: the peak positions and well-width distribution are all consistent with TA spectra reported for PQWs synthesized using smaller A′ cations and with known crystal structures.[41] However, we note that in the absence of clearer structural data for our materials, we cannot assume that NDIC2 directly incorporates into the lattice. It is possible that the NDIC2 molecules form interlayers between 2D-confined perovskite structures and do not bind in the same fashion as smaller A′ cations like phenethylammonium or butylammonium. For simplicity in our discussions, we will still refer to the structures in the $\langle n \rangle = 5$ (FA/MA) film as PQWs, while noting the possible differences from known crystal structures.

Both films show rapid signal decay following photoexcitation, which is typical for mixed PQWs. This is usually attributed to rapid exciton or charge transfer processes occurring from low- to high-n PQWs, occurring on timescales ranging from less than a picosecond (energy transfer) to 10 s or 100 s of picoseconds (charge transfer).[23,27,44] In the $\langle n \rangle = 5$ (FA/MA) thin films, kinetic traces drawn from the $n = 1$, 2, and 3 bleach peaks (Figure 3b) show that their amplitude decreases by more than 50% in less than 0.5 ps after reaching their maximum. There are similarly fast decays observed in the peaks of the PEA-based film (Figure 3d), but the overall amplitude change of these decays is much less by comparison. We posited that the larger decay amplitude in the NDIC2-perovskite hybrids may be indicative of additional ultrafast decay channels induced by electronically coupled NDIC2 compared to the insulating PEA. The transfer of carriers from the photoexcited perovskite to NDIC2 would explain the quenched PL and the difference in carrier dynamics observed here. However, isolating such an ultrafast decay channel is difficult in mixed PQW thin films because of the ubiquitous rapid photoinduced energy and charge transfer processes in these systems.

We instead turned to the $(NDIC2)MA_{(n-1)}Pb_nI_{3n+1}$ (no FA) thin films, where the formation of low-n PQWs appeared inhibited in absorption spectra, potentially offering a system to study the carrier dynamics between the perovskite and NDIC2 without competing carrier transfer processes between wells. We first examined the TA spectra for the $\langle n \rangle = 5$ (MA) film, shown in Figure 4a. At a delay time of 0.3 ps, we can resolve PIA signals from NDIC2 on the high energy side of the spectrum (∼475−600 nm), two small amplitude bleach peaks (∼575 and 610 nm), one central bandedge bleach peak (∼675 nm), and a lower energy PIA (∼710 nm). The bleach peaks at 575 nm and 610 nm are at similar energies to $n = 2$ and $n = 3$ PQWs, and the disappearance of their amplitudes within the first 2 ps may be expected considering the similar dynamics of the PQW signals observed in the $\langle n \rangle = 5$ (FA/MA) films. The lower energy PIA signal, red-shifted relative to the bandedge bleach, has been observed for the above band gap photoexcitation in 3D perovskites,[49] PQWs,[50] and perovskite nanocrystals (or QDs).[51] This peak and its dynamics are attributed to the cooling of hot-carrier distributions and band gap renormalization, which occur within the first few ps following the high energy pump pulse. The red-shifting and narrowing of the initially broad bandedge bleach within the first few ps is also found to occur following above band gap photoexcitation in 3D and quantum-confined perovskites. The bandedge bleach is at a higher energy than that of $MAPbI_3$, suggesting quantum confinement. Notably, the lower energy PIA shifts follows the bandedge bleach as $\langle n \rangle$ is varied (Figure S7), further supporting that these are quantum-confined perovskite structures.

We then compared TA spectra at 2 ps, where any narrowing and red-shifting of the bandedge bleach peak have already occurred, for the other $\langle n \rangle$ films (Figure 4b). The $\langle n \rangle = 4-6$ films exhibit a single bleach peak at ∼675 nm, whereas $\langle n \rangle = 7$ and 8 exhibit an additional bleach peak centered at ∼725 nm. Both of these peaks are blue-shifted relative to the bandedge bleach peak of $MAPbI_3$ (∼750 nm), which may indicate quantum confinement: we have previously observed bleach peaks that are slightly but distinctly blue-shifted by <10 nm for films of $\langle n \rangle = 40$, showing that even weak confinement can still manifest itself in TA spectra.[41] As with the $\langle n \rangle = 5$ film, spectra at earlier delay times for all films (Figure S7) show bleach peaks at wavelengths corresponding to the exciton resonances of $n = 2$ and 3 PQWs, but their amplitudes are at least 10-fold lower than that of the bandedge bleach peak, in agreement

https://dx.doi.org/10.1021/acs.jpcc.0c05521
J. Phys. Chem. C XXXX, XXX, XXX−XXX

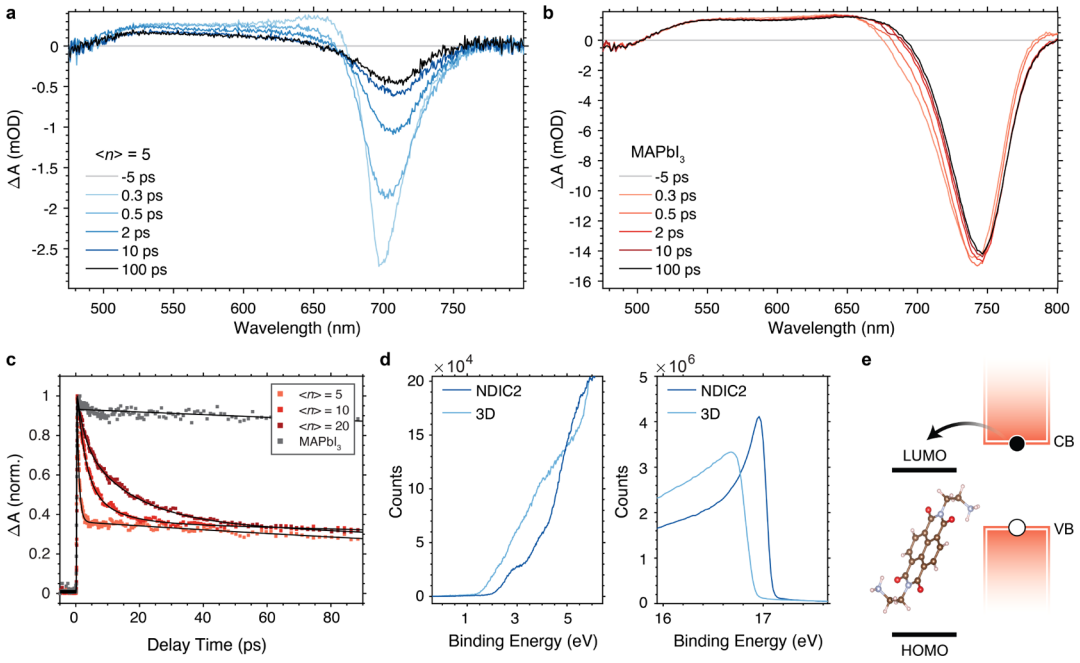

Figure 5. (a) Transient absorption spectra at various delay times for $\langle n \rangle$ = 5 (MA) and (b) $MAPbI_3$ thin films following photoexcitation at a wavelength of 680 nm. (c) Kinetic traces taken from the central wavelength of the bandedge bleach peaks of the $\langle n \rangle$ = 5, 10, and 20 and $MAPbI_3$ films. Full spectra at the same delay times as shown in panel a are shown in Figure S7. (d) UPS spectra for thin films of isolated NDIC2-I_2 and $MAPbI_3$. (e) Proposed band alignment between the perovskite structures and the NDIC2 dication.

with the suppression of low-n well formation we observed in UV−Vis absorption spectra. For higher $\langle n \rangle$, these peaks appear narrower, consistent with reduced disorder with decreasing NDIC2.

The position of the higher energy bleach peak (~675 nm) is close in energy to n = 5 and 6 PQWs, which exhibit bleach peaks at ~660 and ~680 nm, respectively. However, these peaks appear to be broader than usually observed for such systems, which may arise because of slightly different environments or variations in A′-site cation coverage of the structures, causing inhomogeneous broadening. This disorder may be expected considering the broad and low-intensity diffraction of the (110) $MAPbI_3$ peak in XRD patterns.

An alternative explanation is that the blue-shifted bleach peaks instead arise from three-dimensional rather than two-dimensional confinement, forming quantum dot (QD) structures instead of 2D layered structures. However, in this case, we would expect a greater degree of inhomogeneity in the QD size distribution, meaning the bleach peak maximum should gradually shift to lower energies with decreasing NDIC2 content, whereas instead we observe that the bleach peak maxima transition between discrete wavelengths. This observation of fixed peak wavelengths is even more striking when a precursor solvent mixture of dimethyl sulfoxide (DMSO) and γ-butyrolactone (GBL) is used instead of dimethylformamide (DMF), as shown in Figure 4c, where there is a clear separation between a pronounced bleach peak at ~675 nm and another peak at ~740 nm, rather than a continuous, inhomogenously broadened peak spanning these wavelengths. When TA spectra were collected with laser pulses impinging on the back (substrate) side of the film, the higher energy (stronger confinement) peak becomes more pronounced, and the lower energy peak diminished. Notably, similar observations have been made for PQW thin films prepared using butylammonium, where low-n wells form closer to the substrate and high-n wells or 3D perovskite form closer to the surface.[27] This can be understood as a result of lower-n wells consuming more A′ molecules as they form closer to the substrate, depleting their concentration in the rest of the film and leading to higher-n well formation closer to the surface.

We note that some of the recently reported 0D and 1D materials formed from PbI_2 and NDIC2-I_2 had a red coloration attributed to iodide-to-NDIC2 charge transfer.[38] However, it would be unlikely that such a transition would explain the bleach peaks observed in our films because the lower energy PIA dynamics are more consistent with hot-carrier cooling in a quantum-confined perovskite material. It is more likely that if 1D structures form in our films, they do not exhibit iodide-to-NDIC2 charge transfer, but instead absorb at higher energies outside of the window probed here.

We therefore posit that the (NDIC2)$MA_{(n-1)}Pb_nI_{3n+1}$ films consist of a highly disordered mixture of weakly quantum-confined perovskite structures and possibly 1D structures interspersed throughout that are not populated by the photoexcitation pulses in our TA experiments. While the early-time carrier dynamics are highly suggestive of a quantum-confined perovskite structure, the structural disorder and absence of diffraction peaks prevent a definitive assignment of dimensionality, that is, 2D or 3D. Future studies will be required to understand how the combination of NDIC2 and MA cations appears to favor 1D-like structures and inhibit low-n PQW formation, whereas substituting MA with FA appears to negate this effect.

However, despite our uncertainty with regards to its structure, it is still logical to assume that the quantum-confined perovskite materials are either ligated by the NDIC2 molecules or the NDIC2 molecules are localized at the perovskite surfaces because their ability to induce PQW formation was evident in the FA/MA films. The (NDIC2)-$MA_{(n-1)}Pb_nI_{3n+1}$ films thereby offered a platform where the

https://dx.doi.org/10.1021/acs.jpcc.0c05521
J. Phys. Chem. C XXXX, XXX, XXX−XXX

Table 1. Fitting Parameters for Kinetic Traces at Bandedge Exciton Bleach Peaks

sample	λ (nm)	A_1	A_2	A_3	T_1 (ps)	T_2 (ps)	T_3 (ps)
$\langle n \rangle$ = 5	720	0.79 ± 0.02	0.36 ± 0.01	-	0.68 ± 0.02	333 ± 29	-
$\langle n \rangle$ = 10	745	0.61 ± 0.01	0.39 ± 0.01	-	3.3 ± 0.1	316 ± 41	-
$\langle n \rangle$ = 20	750	0.24 ± 0.03	0.41 ± 0.03	0.36 ± 0.04	2.5 ± 0.4	16 ± 3.2	500 ± 300
$MAPbI_3$	765	0.93 ± 0.01	-	-	1313 ± 230	-	-

carrier dynamics of the perovskite could be studied in the presence of NDIC2 and in the absence of other mixed dimensional PQWs. We performed TA spectroscopy with a photoexcitation wavelength of 680 nm, far below the absorption edge of the NDIC2 and close to the bandedge for the perovskite structures (according to the bleach peak in TA spectra). Low excitation fluences were maintained in order to avoid Auger recombination, exciton−exciton annihilation, and two-photon absorption by NDIC2.

TA spectra at various delay times for an $\langle n \rangle$ = 5 (MA) or (NDIC2)$MA_4Pb_5I_{16}$ film, as well as an $MAPbI_3$ reference, are shown in Figure 5a,b. For the $\langle n \rangle$ = 5 (MA) film, the bleach peak is narrower and slightly red-shifted when photoexcited at 680 nm compared to 400 nm (Figure S8), which potentially indicates selective photoexcitation of a subpopulation of the perovskite structures. The perovskite bandedge exciton bleach signal decays rapidly within the first few ps following photoexcitation. This ultrafast decay in signal amplitude does not occur in the $MAPbI_3$ sample, which remains nearly constant at most wavelengths during the first 100 ps. Comparing the spectra in the range of 500 and 650 nm, we see that PIA signals have a slightly higher amplitude at higher energies for the $\langle n \rangle$ = 5 film, whereas the opposite is true for $MAPbI_3$. This occurs in the same region as PIA signals derived from the NDIC2, despite our pump pulse being far detuned from the molecule's absorption. We conducted similar experiments on another set of (NDIC2)$MA_{(n-1)}Pb_nI_{3n+1}$ films with nominal $\langle n \rangle$ values of 5, 10, and 20, shown in Figure S9. In all cases, we observe a rapid decay of the perovskite bleach signal, which becomes slower with increasing $\langle n \rangle$. Because of the overlapping PIA signals from the perovskite, we normalized the TA spectra to their most negative value at each delay time to reveal a relative growth in signal amplitude between 500 and 650 nm, the same region as the NDIC2 PIA signals. This growth occurs on the same timescale as the decay of the perovskite bleach and is not observed for the $MAPbI_3$ film (Figure S10). These dynamics are consistent with carrier transfer from the perovskite to NDIC2—and this would explain our observation of completely quenched emission from the NDIC2-perovskite hybrids compared to $MAPbI_3$. Notably, identical dynamics are obtained in films with and without an XRD peak at 8° (Figure S11). This indicates that the transformation of the 1D structures does not affect the dynamics and they are electronically innocuous in the dynamics observed here, further supporting that NDIC2 is the source of the new decay channel.

Signals originating from NDIC2 appear to be weak in comparison to signals from the perovskite. Gélvez-Rueda et al. observed similar dynamics in TA experiments performed on colloidal PQWs with perylenediimide (PDI) molecules anchored to the surface: following photoexcitation, the bandedge bleach peak of the PQWs decayed due to rapid electron transfer to the PDI, yet the signals from the resulting PDI^- anion were of much lower amplitude (~3.3%) compared to the perovskite bleach, despite the authors calculating a transfer efficiency of ~50% and ~90 PDI molecules per PQW.[31] This could be due to lower extinction coefficients of the NDI and PDI molecules compared to the perovskite structures. Alternatively, in the case of our perovskite-NDI hybrids, it could indicate that electrons undergo transfer to the NDI molecule and then undergo another relaxation or deactivation pathway that prevents any build-up of NDI^- anions, diminishing the signals from this species in our TA experiments.

We fit kinetic traces, taken from near the bleach peak maximum for each of the $\langle n \rangle$ = 5, 10, and 20, and $MAPbI_3$ films, with bi- and triexponential functions. Fitting details and results are shown in Table 1, and the raw data and fits for the kinetic traces are shown in Figure 5c. The decay of the $MAPbI_3$ reference can be well approximated by a single exponential with a time constant greater than 1000 ps when the traces are drawn from the red side of the exciton bleach. We note some shifting of the bandedge bleach within the first few ps following photoexcitation, but otherwise observe that the rest of the spectrum remains essentially constant. The $\langle n \rangle$ = 5 and 10 films exhibit new, much shorter time constants in addition to a long lifetime similar to that of the $MAPbI_3$ reference, whereas the $\langle n \rangle$ = 20 films required triexponential fits which retrieved two time constants in the range of a few picoseconds. We confirmed that this new rapid decay was independent of excitation fluence (Figure S12).

Notably, all traces decay to roughly the same amplitude (the long-time component amplitude of the fits is between 0.36 and 0.41 in all three cases). If perovskite-to-NDIC2 charge transfer is responsible for this decay, we posit that the carrier transfer rates become sequentially slower with increasing $\langle n \rangle$ as the photogenerated carriers require longer times to diffuse to NDIC2. In the case of $\langle n \rangle$ = 20, it is possible that the perovskite domains have become sufficiently large that we can resolve two separate timescales for carrier migration and injection into NDIC2 for carriers generated near and far from these interfaces. This would be consistent with the extra lifetime required to fit the kinetic traces for this sample. In this scenario, carrier migration within the perovskite domains must be rapid in order to provide similar carrier transfer efficiencies as the $\langle n \rangle$ = 5 and 10 films.

We sought to understand the energy level alignment between NDIC2 and the perovskite in order to further support our picture of electron transfer. NDI molecules typically exhibit HOMO (highest occupied molecular orbital) energy levels between −7.5 and −7.0 eV and LUMO (lowest unoccupied molecular orbital) levels in the range of −3.8 to −4.2 eV, estimated using cyclic voltammetry and supported by density functional theory calculations.[52−56] In comparison, the conduction band minimum (CBM) and valence band maximum (VBM) energies for $MAPbI_3$ have been consistently measured to be ~−3.6 and −5.2 eV, respectively.[57−59] We performed ultraviolet photoelectron spectroscopy (UPS) measurements on thin films of the NDIC2 salt and $MAPbI_3$, where we also observe a deeper HOMO level in the NDIC2-I_2

https://dx.doi.org/10.1021/acs.jpcc.0c05521
J. Phys. Chem. C XXXX, XXX, XXX−XXX

film compared to the VBM of $MAPbI_3$ (Figure 5d). We note that it is also likely that the first ionization in the NDIC2-I_2 film is from the iodide counterion, rather than the NDI molecule itself, and that actual NDIC2 dication HOMO is even deeper. $MAPbI_3$ serves as a good reference for the perovskite-like structures in the MA films because the weak confinement is likely not sufficiently strong to substantially shift the bandedge energies. Moreover, we have previously found that energy bands of low-n PQWs can often be even higher in energy than those of $MAPbI_3$ (depending on the surface A′-site cation coverage) and would therefore not impede electron transfer.[60] As the HOMO levels for NDIC2 are deeper in energy than the VBM of $MAPbI_3$, and considering the literature values for LUMO and CBM energies of NDIC2 and $MAPbI_3$, respectively, we find further support for our assignment of transfer of electrons to NDIC2 from the photoexcited perovskite (Figure 5e).

We posit that the dynamics observed between these quantum-confined structures and NDIC2 also occur in the $\langle n \rangle = 5$ (MA/FA) films, explaining the ultrafast decay of signal amplitude for the PQW-like structures. Stronger confinement of such structures ensures a higher CBM energy, which would not impede electron transfer to NDIC2. The rates of charge transfer we observe here are much faster than those typically observed between PQWs, which are on the order of 10−100 s of ps,[23,27] and may arise due to the close proximity of the NDIC2 orbitals to those of the perovskite. We obtain an electron transfer time constant of ∼700 fs for the $\langle n \rangle = 5$ film, compared to ∼16 ps reported for PDI-PQW hybrids.[31] This may suggest a greater electronic coupling between perovskite and NDI molecules compared to PDI molecules or may simply be a consequence of our systems being thin films in solid state, as opposed to colloids in solution. Future studies using a monofunctionalized NDI cation capable of stabilizing colloidal PQWs might further help clarify the photoinduced dynamics observed here, as well as the influence of solid versus solution phase.

Following electron transfer, the electrons and holes may be strongly localized on the NDIC2 dications and perovskite structures, respectively, as in colloidal PDI-PQW hybrids;[31] although this requires the assumption that the NDI^- is not immediately deactivated after its formation. Electron−hole pairs that remain strongly bound across heterojunction interfaces, also called charge-transfer states, can have significant oscillator strengths that usually result in broad, red-shifted PIA signals.[61−63] We observe no such signals in any of our TA spectra. Zhao et al. have demonstrated the existence and direct absorption of donor/acceptor charge transfer states between 2D ($n = 1$) PQWs and organic electron acceptor molecules in external quantum efficiency measurements, but these states are absent when $n = 2$ or $n = 3$ perovskites are employed instead of $n = 1$, possibly indicating that low dimensionality is required to facilitate appreciable binding of the carriers in a PQW-organic charge transfer excited state.[64]

To conclude, in this study of NDIC2 A′-site dications on the structural and optical properties of reduced-dimensional perovskites in thin films, we find that—compared to perovskite structures synthesized with smaller alkyl- or arylammonium cations—the NDIC2 dication results in weakly confined perovskite structures and 1D complexes when only methylammonium is used as a A-site cation, inhibiting the formation of PQWs. When formamidinium is used instead, dimensionally and spatially inhomogeneous PQW-like structures are obtained. In ultrafast transient absorption spectroscopy experiments, we observe a rapid (∼700 fs) decay of perovskite signals in the presence of NDIC2, which is consistent with perovskite-to-NDIC2 charge transfer. This work demonstrates the unusual influence of the A′- and A-site cations on the resulting perovskite structure and the potential utility of such molecules to capture carriers from the perovskite on ultrafast timescales.

■ ASSOCIATED CONTENT

Supporting Information

The Supporting Information is available free of charge at https://pubs.acs.org/doi/10.1021/acs.jpcc.0c05521.

Materials, table of precusor ratios; ^{1}H-NMR spectra; transient absorption spectra; XRD patterns; and fluence-dependent kinetic traces (PDF)

■ AUTHOR INFORMATION

Corresponding Author

Edward H. Sargent − *The Edward S. Rogers Department of Electrical and Computer Engineering, University of Toronto, Toronto, Ontario M5S 3G4, Canada;* orcid.org/0000-0003-0396-6495; Email: ted.sargent@utoronto.ca

Authors

Andrew H. Proppe − *Department of Chemistry and The Edward S. Rogers Department of Electrical and Computer Engineering, University of Toronto, Toronto, Ontario M5S 3G4, Canada;* orcid.org/0000-0003-3860-9949

Marie-Hélène Tremblay − *Center for Organic Photonics and Electronics, School of Chemistry and Biochemistry, Georgia Institute of Technology, Atlanta, Georgia 30332-0400, United States*

Yadong Zhang − *Center for Organic Photonics and Electronics, School of Chemistry and Biochemistry, Georgia Institute of Technology, Atlanta, Georgia 30332-0400, United States*

Zhenyu Yang − *The Edward S. Rogers Department of Electrical and Computer Engineering, University of Toronto, Toronto, Ontario M5S 3G4, Canada;* orcid.org/0000-0002-6403-8679

Rafael Quintero-Bermudez − *The Edward S. Rogers Department of Electrical and Computer Engineering, University of Toronto, Toronto, Ontario M5S 3G4, Canada;* orcid.org/0000-0002-4233-395X

Shana O. Kelley − *Department of Chemistry and Department of Pharmaceutical Sciences, Leslie Dan Faculty of Pharmacy, University of Toronto, Toronto, Ontario M5S 3G4, Canada;* orcid.org/0000-0003-3360-5359

Stephen Barlow − *Center for Organic Photonics and Electronics, School of Chemistry and Biochemistry, Georgia Institute of Technology, Atlanta, Georgia 30332-0400, United States;* orcid.org/0000-0001-9059-9974

Seth R. Marder − *Center for Organic Photonics and Electronics, School of Chemistry and Biochemistry, Georgia Institute of Technology, Atlanta, Georgia 30332-0400, United States;* orcid.org/0000-0001-6921-2536

Complete contact information is available at: https://pubs.acs.org/10.1021/acs.jpcc.0c05521

Notes

The authors declare no competing financial interest.

https://dx.doi.org/10.1021/acs.jpcc.0c05521
J. Phys. Chem. C XXXX, XXX, XXX−XXX

■ ACKNOWLEDGMENTS

This publication is partly based on work supported by the United States Department of the Navy, Office of Naval Research (grant award no.: N00014-17-1-2524) and the United States Air Force Office of Scientific Research (FA9550-18-1-0499). The authors thank the Ontario Graduate Scholarship program (A.H.P.) and the Natural Sciences and Engineering Research Council of Canada (A.H.P. and M.-H.T.). This work was performed in part at the Georgia Tech Institute for Electronics and Nanotechnology, a member of the National Nanotechnology Coordinated Infrastructure, which is supported by the National Science Foundation (Grant ECCS-1542174). This work was performed in part at the Georgia Tech NMR Center and the CSICOMP NMR Facility at the University of Toronto.

■ REFERENCES

(1) Wang, Z.; Lin, Q.; Chmiel, F. P.; Sakai, N.; Herz, L. M.; Snaith, H. J. Efficient Ambient-Air-Stable Solar Cells with 2D−3D Heterostructured Butylammonium-Caesium-Formamidinium Lead Halide Perovskites. *Nat. Energy* **2017**, *2*, 17135.

(2) Christians, J. A.; Schulz, P.; Tinkham, J. S.; Schloemer, T. H.; Harvey, S. P.; Tremolet de Villers, B. J.; Sellinger, A.; Berry, J. J.; Luther, J. M. Tailored Interfaces of Unencapsulated Perovskite Solar Cells for >1,000 Hour Operational Stability. *Nat. Energy* **2018**, *3*, 68.

(3) Hou, Y.; Du, X.; Scheiner, S.; McMeekin, D. P.; Wang, Z.; Li, N.; Killian, M. S.; Chen, H.; Richter, M.; Levchuk, I.; et al. A Generic Interface to Reduce the Efficiency-Stability-Cost Gap of Perovskite Solar Cells. *Science* **2017**, *358*, 1192−1197.

(4) Jeon, N. J.; Na, H.; Jung, E. H.; Yang, T.-Y.; Lee, Y. G.; Kim, G.; Shin, H.-W.; Il Seok, S.; Lee, J.; Seo, J. A Fluorene-Terminated Hole-Transporting Material for Highly Efficient and Stable Perovskite Solar Cells. *Nat. Energy* **2018**, *3*, 682−689.

(5) Jeon, N. J.; Noh, J. H.; Yang, W. S.; Kim, Y. C.; Ryu, S.; Seo, J.; Seok, S. I. Compositional Engineering of Perovskite Materials for High-Performance Solar Cells. *Nature* **2015**, *517*, 476−480.

(6) Jung, E. H.; Jeon, N. J.; Park, E. Y.; Moon, C. S.; Shin, T. J.; Yang, T.-Y.; Noh, J. H.; Seo, J. Efficient, Stable and Scalable Perovskite Solar Cells Using Poly(3-Hexylthiophene). *Nature* **2019**, *567*, 511.

(7) Jiang, Q.; Chu, Z.; Wang, P.; Yang, X.; Liu, H.; Wang, Y.; Yin, Z.; Wu, J.; Zhang, X.; You, J. Planar-Structure Perovskite Solar Cells with Efficiency beyond 21%. *Adv. Mater.* **2017**, *29*, 1703852.

(8) Tsai, H.; Nie, W.; Blancon, J.-C.; Stoumpos, C. C.; Asadpour, R.; Harutyunyan, B.; Neukirch, A. J.; Verduzco, R.; Crochet, J. J.; Tretiak, S.; et al. High-efficiency two-dimensional Ruddlesden-Popper perovskite solar cells. *Nature* **2016**, *536*, 312−316.

(9) Zhang, X.; Ren, X.; Liu, B.; Munir, R.; Zhu, X.; Yang, D.; Li, J.; Liu, Y.; Smilgies, D.-M.; Li, R.; et al. Stable High Efficiency Two-Dimensional Perovskite Solar Cells via Cesium Doping. *Energy Environ. Sci.* **2017**, *10*, 2095−2102.

(10) Cao, D. H.; Stoumpos, C. C.; Farha, O. K.; Hupp, J. T.; Kanatzidis, M. G. 2D Homologous Perovskites as Light-Absorbing Materials for Solar Cell Applications. *J. Am. Chem. Soc.* **2015**, *137*, 7843−7850.

(11) Soe, C. M. M.; Stoumpos, C. C.; Kepenekian, M.; Traoré, B.; Tsai, H.; Nie, W.; Wang, B.; Katan, C.; Seshadri, R.; Mohite, A. D.; et al. New Type of 2D Perovskites with Alternating Cations in the Interlayer Space, (C(NH2)3)(CH3NH3)nPbnI3n+1: Structure, Properties, and Photovoltaic Performance. *J. Am. Chem. Soc.* **2017**, *139*, 16297−16309.

(12) Stoumpos, C. C.; Cao, D. H.; Clark, D. J.; Young, J.; Rondinelli, J. M.; Jang, J. I.; Hupp, J. T.; Kanatzidis, M. G. Ruddlesden-Popper Hybrid Lead Iodide Perovskite 2D Homologous Semiconductors. *Chem. Mater.* **2016**, *28*, 2852−2867.

(13) Ishihara, T.; Takahashi, J.; Goto, T. Exciton state in two-dimensional perovskite semiconductor (C10H21NH3)2PbI4. *Solid State Commun.* **1989**, *69*, 933−936.

(14) Hong, X.; Ishihara, T.; Nurmikko, A. V. Dielectric confinement effect on excitons inPbI4-based layered semiconductors. *Phys. Rev. B: Condens. Matter Mater. Phys.* **1992**, *45*, 6961−6964.

(15) Elkins, M. H.; Pensack, R.; Proppe, A. H.; Voznyy, O.; Quan, L. N.; Kelley, S. O.; Sargent, E. H.; Scholes, G. D. Biexciton Resonances Reveal Exciton Localization in Stacked Perovskite Quantum Wells. *J. Phys. Chem. Lett.* **2017**, *8*, 3895−3901.

(16) Wang, N.; Cheng, L.; Ge, R.; Zhang, S.; Miao, Y.; Zou, W.; Yi, C.; Sun, Y.; Cao, Y.; Yang, R.; et al. Perovskite Light-Emitting Diodes Based on Solution-Processed Self-Organized Multiple Quantum Wells. *Nat. Photonics* **2016**, *10*, 699−704.

(17) Wu, X.; Trinh, M. T.; Zhu, X.-Y. Excitonic Many-Body Interactions in Two-Dimensional Lead Iodide Perovskite Quantum Wells. *J. Phys. Chem. C* **2015**, *119*, 14714−14721.

(18) Trinh, M. T.; Wu, X.; Niesner, D.; Zhu, X.-Y. Many-Body Interactions in Photo-Excited Lead Iodide Perovskite. *J. Mater. Chem. A* **2015**, *3*, 9285−9290.

(19) Even, J.; Pedesseau, L.; Katan, C. Understanding Quantum Confinement of Charge Carriers in Layered 2D Hybrid Perovskites. *ChemPhysChem* **2014**, *15*, 3733−3741.

(20) Kamminga, M. E.; Fang, H.-H.; Filip, M. R.; Giustino, F.; Baas, J.; Blake, G. R.; Loi, M. A.; Palstra, T. T. M. Confinement Effects in Low-Dimensional Lead Iodide Perovskite Hybrids. *Chem. Mater.* **2016**, *28*, 4554−4562.

(21) Quan, L. N.; Yuan, M.; Comin, R.; Voznyy, O.; Beauregard, E. M.; Hoogland, S.; Buin, A.; Kirmani, A. R.; Zhao, K.; Amassian, A.; et al. Ligand-Stabilized Reduced-Dimensionality Perovskites. *J. Am. Chem. Soc.* **2016**, *138*, 2649−2655.

(22) Proppe, A. H.; Quintero-Bermudez, R.; Tan, H.; Voznyy, O.; Kelley, S. O.; Sargent, E. H. Synthetic Control over Quantum Well Width Distribution and Carrier Migration in Low-Dimensional Perovskite Photovoltaics. *J. Am. Chem. Soc.* **2018**, *140*, 2890−2896.

(23) Proppe, A. H.; Elkins, M. H.; Voznyy, O.; Pensack, R. D.; Zapata, F.; Besteiro, L. V.; Quan, L. N.; Quintero-Bermudez, R.; Todorovic, P.; Kelley, S. O.; et al. Spectrally Resolved Ultrafast Exciton Transfer in Mixed Perovskite Quantum Wells. *J. Phys. Chem. Lett.* **2019**, *10*, 419−426.

(24) Peng, W.; Yin, J.; Ho, K.-T.; Ouellette, O.; De Bastiani, M.; Murali, B.; El Tall, O.; Shen, C.; Miao, X.; Pan, J.; et al. Ultralow Self-Doping in Two-Dimensional Hybrid Perovskite Single Crystals. *Nano Lett.* **2017**, *17*, 4759−4767.

(25) Yuan, M.; Quan, L. N.; Comin, R.; Walters, G.; Sabatini, R.; Voznyy, O.; Hoogland, S.; Zhao, Y.; Beauregard, E. M.; Kanjanaboos, P.; et al. Perovskite Energy Funnels for Efficient Light-Emitting Diodes. *Nat. Nanotechnol.* **2016**, *11*, 872−877.

(26) He, Z.; Liu, Y.; Yang, Z.; Li, J.; Cui, J.; Chen, D.; Fang, Z.; He, H.; Ye, Z.; Zhu, H.; et al. High-Efficiency Red Light-Emitting Diodes Based on Multiple Quantum Wells of Phenylbutylammonium-Cesium Lead Iodide Perovskites. *ACS Photonics* **2019**, *6*, 587.

(27) Liu, J.; Leng, J.; Wu, K.; Zhang, J.; Jin, S. Observation of Internal Photoinduced Electron and Hole Separation in Hybrid Two-Dimentional Perovskite Films. *J. Am. Chem. Soc.* **2017**, *139*, 1432−1435.

(28) Mitzi, D. B.; Chondroudis, K.; Kagan, C. R. Design, Structure, and Optical Properties of Organic−Inorganic Perovskites Containing an Oligothiophene Chromophore. *Inorg. Chem.* **1999**, *38*, 6246−6256.

(29) Chondroudis, K.; Mitzi, D. B. Electroluminescence from an Organic−Inorganic Perovskite Incorporating a Quaterthiophene Dye within Lead Halide Perovskite Layers. *Chem. Mater.* **1999**, *11*, 3028−3030.

(30) Passarelli, J. V.; Fairfield, D. J.; Sather, N. A.; Hendricks, M. P.; Sai, H.; Stern, C. L.; Stupp, S. I. Enhanced Out-of-Plane Conductivity and Photovoltaic Performance in n = 1 Layered Perovskites through Organic Cation Design. *J. Am. Chem. Soc.* **2018**, *140*, 7313−7323.

(31) Gélvez-Rueda, M. C.; Fridriksson, M. B.; Dubey, R. K.; Jager, W. F.; van der Stam, W.; Grozema, F. C. Overcoming the Exciton

https://dx.doi.org/10.1021/acs.jpcc.0c05521
J. Phys. Chem. C XXXX, XXX, XXX−XXX

Binding Energy in Two-Dimensional Perovskite Nanoplatelets by Attachment of Conjugated Organic Chromophores. *Nat. Commun.* **2020**, *11*, 1901.
(32) Gélvez-Rueda, M. C.; Van Gompel, W. T. M.; Herckens, R.; Lutsen, L.; Vanderzande, D.; Grozema, F. C. Inducing Charge Separation in Solid-State Two-Dimensional Hybrid Perovskites through the Incorporation of Organic Charge-Transfer Complexes. *J. Phys. Chem. Lett.* **2020**, *11*, 824−830.
(33) Passarelli, J. V.; Mauck, C. M.; Winslow, S. W.; Perkinson, C. F.; Bard, J. C.; Sai, H.; Williams, K. W.; Narayanan, A.; Fairfield, D. J.; Hendricks, M. P.; et al. Tunable exciton binding energy in 2D hybrid layered perovskites through donor-acceptor interactions within the organic layer. *Nat. Chem.* **2020**, *12*, 672−682.
(34) Licchelli, M.; Linati, L.; Orbelli Biroli, A.; Perani, E.; Poggi, A.; Sacchi, D. Metal-Induced Assembling/Disassembling of Fluorescent Naphthalenediimide Derivatives Signalled by Excimer Emission. *Chem.—Eur. J.* **2002**, *8*, 5161−5169.
(35) Li, X.; Yang, J.; Song, Z.; Chen, R.; Ma, L.; Li, H.; Jia, J.; Meng, J.; Li, X.; Yi, M.; et al. Naphthalene Diimide Ammonium Directed Single-Crystalline Perovskites with "Atypical" Ambipolar Charge Transport Signatures in Two-Dimensional Limit. *ACS Appl. Energy Mater.* **2018**, *1*, 4467−4472.
(36) Liu, J.-J.; Guan, Y.-F.; Jiao, C.; Lin, M.-J.; Huang, C.-C.; Dai, W.-X. A Panchromatic Hybrid Crystal of Iodoplumbate Nanowires and J-Aggregated Naphthalene Diimides with Long-Lived Charge-Separated States. *Dalton Trans.* **2015**, *44*, 5957−5960.
(37) Liu, J.-J.; Chen, Y.; Lin, M.-J.; Huang, C.-C.; Dai, W.-X. Two-Semiconductive-Component Hybrid Coordination Polymers with Controllable Photo-Induced Electron-Transfer Properties. *Dalton Trans.* **2016**, *45*, 6339−6342.
(38) Tremblay, M.-H.; Zeidell, A. M.; Rigin, S.; Tyznik, C.; Bacsa, J.; Zhang, Y.; Al Kurdi, K.; Jurchescu, O. D.; Timofeeva, T. V.; Barlow, S.; et al. Structural Diversity in 2,2′-[Naphthalene-1,8:4,5-Bis-(Dicarboximide)-N,N′-Diyl]-Bis(Ethylammonium) Iodoplumbates. *Inorg. Chem.* **2020**, *59*, 8070.
(39) Sheldrick, G. M. SHELXT- Integrated space-group and crystal-structure determination. *Acta Crystallogr., Sect. A: Found. Adv.* **2015**, *71*, 3−8.
(40) Sheldrick, G. M. Crystal structure refinement withSHELXL. *Acta Crystallogr., Sect. C: Struct. Chem.* **2015**, *71*, 3−8.
(41) Quintero-Bermudez, R.; Gold-Parker, A.; Proppe, A. H.; Munir, R.; Yang, Z.; Kelley, S. O.; Amassian, A.; Toney, M. F.; Sargent, E. H. Compositional and Orientational Control in Metal Halide Perovskites of Reduced Dimensionality. *Nat. Mater.* **2018**, *17*, 900.
(42) Shi, D.; Adinolfi, V.; Comin, R.; Yuan, M.; Alarousu, E.; Buin, A.; Chen, Y.; Hoogland, S.; Rothenberger, A.; Katsiev, K.; et al. Low Trap-State Density and Long Carrier Diffusion in Organolead Trihalide Perovskite Single Crystals. *Science* **2015**, *347*, 519−522.
(43) Mao, L.; Ke, W.; Pedesseau, L.; Wu, Y.; Katan, C.; Even, J.; Wasielewski, M. R.; Stoumpos, C. C.; Kanatzidis, M. G. Hybrid Dion-Jacobson 2D Lead Iodide Perovskites. *J. Am. Chem. Soc.* **2018**, *140*, 3775−3783.
(44) Shang, Q.; Wang, Y.; Zhong, Y.; Mi, Y.; Qin, L.; Zhao, Y.; Qiu, X.; Liu, X.; Zhang, Q. Unveiling Structurally Engineered Carrier Dynamics in Hybrid Quasi-Two-Dimensional Perovskite Thin Films toward Controllable Emission. *J. Phys. Chem. Lett.* **2017**, *8*, 4431−4438.
(45) Gosztola, D.; Niemczyk, M. P.; Svec, W.; Lukas, A. S.; Wasielewski, M. R. Excited Doublet States of Electrochemically Generated Aromatic Imide and Diimide Radical Anions. *J. Phys. Chem. A* **2000**, *104*, 6545−6551.
(46) Bélanger-Chabot, G.; Ali, A.; Gabbaï, F. P. On the Reaction of Naphthalene Diimides with Fluoride Ions: Acid/Base versus Redox Reactions. *Angew. Chem.* **2017**, *129*, 10090−10093.
(47) Bhosale, S. V.; Jani, C. H.; Langford, S. J. Chemistry of Naphthalene Diimides. *Chem. Soc. Rev.* **2008**, *37*, 331−342.
(48) Dawson, R. E.; Hennig, A.; Weimann, D. P.; Emery, D.; Ravikumar, V.; Montenegro, J.; Takeuchi, T.; Gabutti, S.; Mayor, M.; Mareda, J.; et al. Experimental evidence for the functional relevance of anion-π interactions. *Nat. Chem.* **2010**, *2*, 533−538.
(49) Price, M. B.; Butkus, J.; Jellicoe, T. C.; Sadhanala, A.; Briane, A.; Halpert, J. E.; Broch, K.; Hodgkiss, J. M.; Friend, R. H.; Deschler, F. Hot-Carrier Cooling and Photoinduced Refractive Index Changes in Organic−Inorganic Lead Halide Perovskites. *Nat. Commun.* **2015**, *6*, 8420.
(50) Giovanni, D.; Chong, W. K.; Liu, Y. Y. F.; Dewi, H. A.; Yin, T.; Lekina, Y.; Shen, Z. X.; Mathews, N.; Gan, C. K.; Sum, T. C. Coherent Spin and Quasiparticle Dynamics in Solution-Processed Layered 2D Lead Halide Perovskites. *Adv. Sci.* **2018**, *5*, 1800664.
(51) Ashner, M. N.; Shulenberger, K. E.; Krieg, F.; Powers, E. R.; Kovalenko, M. V.; Bawendi, M. G.; Tisdale, W. A. Size-Dependent Biexciton Spectrum in CsPbBr3 Perovskite Nanocrystals. *ACS Energy Lett.* **2019**, *4*, 2639−2645.
(52) Kozycz, L. M.; Guo, C.; Manion, J. G.; Tilley, A. J.; Lough, A. J.; Li, Y.; Seferos, D. S. Enhanced Electron Mobility in Crystalline Thionated Naphthalene Diimides. *J. Mater. Chem. C* **2015**, *3*, 11505−11515.
(53) Rozanski, L. J.; Castaldelli, E.; Sam, F. L. M.; Mills, C. A.; Jean-François Demets, G.; Silva, S. R. P. Solution Processed Naphthalene Diimide Derivative as Electron Transport Layers for Enhanced Brightness and Efficient Polymer Light Emitting Diodes. *J. Mater. Chem. C* **2013**, *1*, 3347−3352.
(54) Uddin, M. A.; Kim, Y.; Younts, R.; Lee, W.; Gautam, B.; Choi, J.; Wang, C.; Gundogdu, K.; Kim, B. J.; Woo, H. Y. Controlling Energy Levels and Blend Morphology for All-Polymer Solar Cells via Fluorination of a Naphthalene Diimide-Based Copolymer Acceptor. *Macromolecules* **2016**, *49*, 6374−6383.
(55) Xiao, B.; Ding, G.; Tan, Z. a.; Zhou, E. A Comparison of N-Type Copolymers Based on Cyclopentadithiophene and Naphthalene Diimide/Perylene Diimides for All-Polymer Solar Cell Applications. *Polym. Chem.* **2015**, *6*, 7594−7602.
(56) Jones, B. A.; Facchetti, A.; Wasielewski, M. R.; Marks, T. J. Tuning Orbital Energetics in Arylene Diimide Semiconductors. Materials Design for Ambient Stability of n-Type Charge Transport. *J. Am. Chem. Soc.* **2007**, *129*, 15259−15278.
(57) Endres, J.; Egger, D. A.; Kulbak, M.; Kerner, R. A.; Zhao, L.; Silver, S. H.; Hodes, G.; Rand, B. P.; Cahen, D.; Kronik, L.; et al. Valence and Conduction Band Densities of States of Metal Halide Perovskites: A Combined Experimental-Theoretical Study. *J. Phys. Chem. Lett.* **2016**, *7*, 2722−2729.
(58) Schulz, P.; Edri, E.; Kirmayer, S.; Hodes, G.; Cahen, D.; Kahn, A. Interface Energetics in Organo-Metal Halide Perovskite-Based Photovoltaic Cells. *Energy Environ. Sci.* **2014**, *7*, 1377−1381.
(59) Hoye, R. L. Z.; Schulz, P.; Schelhas, L. T.; Holder, A. M.; Stone, K. H.; Perkins, J. D.; Vigil-Fowler, D.; Siol, S.; Scanlon, D. O.; Zakutayev, A.; et al. Perovskite-Inspired Photovoltaic Materials: Toward Best Practices in Materials Characterization and Calculations. *Chem. Mater.* **2017**, *29*, 1964−1988.
(60) Quintero-Bermudez, R.; Proppe, A. H.; Mahata, A.; Todorović, P.; Kelley, S. O.; De Angelis, F.; Sargent, E. H. Ligand-Induced Surface Charge Density Modulation Generates Local Type-II Band Alignment in Reduced-Dimensional Perovskites. *J. Am. Chem. Soc.* **2019**, *141*, 13459−13467.
(61) Hwang, I.-W.; Soci, C.; Moses, D.; Zhu, Z.; Waller, D.; Gaudiana, R.; Brabec, C. J.; Heeger, A. J. Ultrafast Electron Transfer and Decay Dynamics in a Small Band Gap Bulk Heterojunction Material. *Adv. Mater.* **2007**, *19*, 2307−2312.
(62) Grancini, G.; Polli, D.; Fazzi, D.; Cabanillas-Gonzalez, J.; Cerullo, G.; Lanzani, G. Transient Absorption Imaging of P3HT:PCBM Photovoltaic Blend: Evidence For Interfacial Charge Transfer State. *J. Phys. Chem. Lett.* **2011**, *2*, 1099−1105.
(63) Siegmund, B.; Mischok, A.; Benduhn, J.; Zeika, O.; Ullbrich, S.; Nehm, F.; Böhm, M.; Spoltore, D.; Fröb, H.; Körner, C.; et al. Organic Narrowband Near-Infrared Photodetectors Based on Intermolecular Charge-Transfer Absorption. *Nat. Commun.* **2017**, *8*, 15421.

https://dx.doi.org/10.1021/acs.jpcc.0c05521
J. Phys. Chem. C XXXX, XXX, XXX−XXX

(64) Zhao, L.; Lin, Y. L.; Kim, H.; Giebink, N. C.; Rand, B. P. Donor/Acceptor Charge-Transfer States at Two-Dimensional Metal Halide Perovskite and Organic Semiconductor Interfaces. *ACS Energy Lett.* **2018**, 3, 2708−2712.

https://dx.doi.org/10.1021/acs.jpcc.0c05521
J. Phys. Chem. C XXXX, XXX, XXX−XXX